Effect of electrolyte concentration on performance of supercapacitor carbon electrode from fibers of oil palm empty fruit bunches

R. Farma, M. Deraman, I. A. Talib, Awitdrus, R. Omar, M. M. Ishak, E. Taer, N. H. Basri, and B. N. M. Dolah

---

Articles you may be interested in

Effect of carbonization temperature on the physical and electrochemical properties of supercapacitor electrode from fibers of oil palm empty fruit bunches
AIP Conf. Proc. **1656**, 030005 (2015); 10.1063/1.4917094

Nanoporous separators for supercapacitor using activated carbon monolith electrode from oil palm empty fruit bunches
AIP Conf. Proc. **1586**, 68 (2014); 10.1063/1.4866732

Production of succinic acid from oil palm empty fruit bunch cellulose using Actinobacillus succinogenes
AIP Conf. Proc. **1571**, 753 (2013); 10.1063/1.4858745

Carbon/Carbon Nanotubes (CNTs) Composites from Green Pellets Contain CNTs and Self-adhesive Carbon Grains from Fibres of Oil Palm Empty Fruit Bunch
AIP Conf. Proc. **1284**, 179 (2010); 10.1063/1.3515546

Effect of Reinforcement Shape and Fiber Treatment on the Mechanical Properties of Oil Palm Empty Fruit Bunch-Polyethylene Composites
AIP Conf. Proc. **1217**, 335 (2010); 10.1063/1.3377839

Effect of Electrolyte Concentration on Performance of Supercapacitor Carbon Electrode from Fibers of Oil Palm Empty Fruit Bunches

R. Farma [1,2], M. Deraman [*,1], I.A. Talib[1], Awitdrus[1,2], R. Omar[1], M.M. Ishak[1], E. Taer[1,2], N.H. Basri[1] and B.N.M. Dolah[1]

[1]School of Applied Physics, Faculty of Science and Technology, Universiti Kebangsaan Malaysia,
43600 Bangi, Selangor, Malaysia
[2]Departement of Physics, Faculty of Mathematics and Natural Sciences, University of Riau,
28293 Pekanbaru, Riau, Indonesia
*Corresponding author. E-mail: madra@ukm.my

Abstract. Fibers of oil palm empty fruit bunches were used to produce self-adhesive carbon grains (SACG). The SACG green monoliths were carbonized in N_2 environment at 800°C to produce carbon monoliths (CM) and the CM was CO_2 activated at 800°C for 4 hour to produce activated carbon monolith electrodes (ACM). The physical properties of the CMs and ACMs were investigated using X-ray diffraction, field emission scanning electron microscopy and nitrogen adsorption-desorption. ACMs were used as electrode to fabricate symmetry supercapacitor cells and the cells which used H_2SO_4 electrolyte at 0.5, 1.0 and 1.5 M were investigated using electrochemical impedance spectroscopy, cyclic voltammetry and galvanostatic charge-discharge standard techniques. In this paper we report the physical properties of the ACM electrodes and the effect of electrolyte concentration on the electrochemical properties the ACM electrodes.

Keywords: *Activated carbon monolith, Porosity, Electrolyte concentration, Supercapacitor, Electrochemical properties.*
PACS: 81.05.U-, 68.43.-h, 82.45.Gj, 82.47.Uv, 84.37.+q

INTRODUCTION

Supercapacitor is an electrochemical energy storage device having electrode, electrolyte (aqueous or organic [1]), current collector and separator as its major components and it can store and release energy rapidly. Its energy and power performance lies between the battery and conventional capacitor. Mechanism of energy storage is based on the concept of double layer that is formed at the electrode-electrolyte interface by ionic charges from electrolyte and electronic charges from electrode. Typical types of material used as supercapacitor electrode are metal oxide, polymer and porous materials such as activated carbon and carbon aerogel. Porous carbon which can be produced from different types of organic materials, i.e. hydrocarbon gas, petroleum, coal, polymers or biomass [2], have been widely used as supercapacitor electrode because it has advantages such as (i) high electrical conductivity, (ii) high surface area, (iii) good corrosion resistance, (iv) high temperature stability, (v) pore structure which can be controlled [3]. Summary of performance of supercapacitor carbon electrodes prepared from different type of biomass materials such as wasted coffee beans, sugar cane bagasse, rice husk, bamboo, rubber wood sawdust, used paper and walnut shell can be found in ref. [4].

The selection of electrolyte solution can influence the capacitance of supercapacitor cells because each electrolyte has its own ionic size, electrical conductivity and working voltage. Commonly used aqueous electrolyte solutions are, for example sulfuric acid [5], sodium sulfate [6], and potassium hydroxide [7] and sodium hydroxide [8] for acidic, neutral and alkaline solutions, respectively. Formation of a double layer is involved the mobility of electrolyte ions into pores of electrode and this mobility will be decreased if a very high concentration of electrolyte is used because in such a condition ions activity is reduced due to less water hydration. However, if electrolyte concentration is too low then there will be insufficient quantity of ionic charges for the double layer. Therefore there have been many studies [5,6,9] to optimize the concentration of electrolyte in order to increase ions transport into pores of electrode, which can lead to an effective formation of double layer that can produce maximum specific capacitance, specific energy and specific power. In the present study, H_2SO_4 electrolyte solution with different concentration of 0.5, 1.0 and 1.5 M were used as an electrolyte in the cells of supercapacitor fabricated using activated

carbon monolith electrodes prepared from biomass materials, i.e. fibers of oil palm empty fruit bunches (EFB).

EXPERIMENTAL

Self adhesive carbon grain (SACG) with particles size ≤106 μm were prepared from EFB by pre-carbonization, milling and sieving [10]. 30 g of SACG were heated in 300 ml of distilled water at 100°C for 1 hour and followed by drying in an oven at 100°C for 48 hours. 10 g of dry powder were milled by a VT-Mini Ring Mill for 20 minutes to obtain fine powder of SACG. 0.75 g SACG was pelletized in a mould with a diameter of 20 mm using a hydraulic press machine (VISITEC 2009-Malaysia) with a compression pressure of 250 kg cm^{-2} to produce green monoliths (GMs). GMs were carbonized at 800°C in a furnace (Vulcan Box Furnace 3-1750) with a multi step heating profile in the N$_2$ environment (1.5 $l$min^{-1}) to produce carbon monoliths (CMs) [10].

CMs were activated using CO$_2$ gas (1.0 $l$min^{-1}) at 800°C for 4 hours with a heating rate of 5°Cmin^{-1} using our previous method to produce activated carbon monoliths (ACMs) [4]. ACMs were polished up to 0.4 mm thickness for an application as supercapacitor electrode. Symmetrical supercapacitor cells were fabricated using ACMs electrodes, 316L stainless steel current collector (thickness of 0.04 mm, Good fellow, England), teflon separator (thickness of 0.2 mm), and sulfuric acid (H$_2$SO$_4$) electrolyte with concentrations of 0.5, 1.0 and 1.5 M, respectively. For convenient, with respect to their respective electrolyte, the supercapacitor cells were labeled as Cell(0.5), Cell(1.0) and Cell(1.5).

The weight (Mettler Toledo AB204) and dimensions (Mitutoyo 193-253) of GMs, CMs and ACMs respectively, were measured to determine their density. The microcrystalites dimension (stack width (L$_{a(100)}$) and stack height (L$_{c(002)}$)) and the interlayers spacing (d$_{002}$ and d$_{100}$) of ACMs were determined using X-ray diffraction (XRD) method (Instrument: Bruker AXS: D8 Advance model). The microstructure of ACMs was investigated using a Field Emission Scanning Electron Microscope (FESEM) (Zeiss SUPRA 55VP). Parameters of porosity characteristic such as BET surface area (S$_{BET}$), micropore surface area(S$_{Micro}$), mesopore surface area (S$_{Meso}$), micropore volume(V$_{Micro}$), mesopore volume (V$_{Meso}$), and average pore diameter (D) of the ACMs were determined from the N$_2$ adsorption-desorption isotherms measurement (77 K) using an Accelerated Surface Area and Porosimeter System (ASAP 2010 Micromeretic).

Characterization of Cell(0.5), Cell(1.0) and Cell(1.5) using electrochemical impedance spectroscopy (EIS), cyclic voltammogram (CV) and

galvanostatic charge-discharge (GCD) methods was conducted using a Solartron 1286 and an electrochemical 1255HF Solartron Interface Frequency Response Analyzer. Specific capacitance of supercapacitor cells was calculated from the EIS, CV and GCD data, respectively, using equations (1), (2) and (3) [11]

$$C_{sp} = -\frac{1}{\pi f Z'' m} \tag{1}$$

$$C_{sp} = \frac{2i}{Sm} \tag{2}$$

$$C_{sp} = \frac{2i'}{\left(\frac{\Delta V}{\Delta t}\right) m} \tag{3}$$

where f is the frequency (Hz), Z'' is the imaginary part of impedance at the lowest frequency, i is the current (A), S is the scan rate (mV/s), ΔV is the voltage-changed (V), Δt is the time-changed (s), i' is the current density (mA/cm^2) and m is the weight of electrode. The specific energy (E) and specific power (P) of the supercapacitor cells were calculated from the discharge curve of the GCD data using equations (4) and (5), respectively [4]

$$E = \frac{Vit}{m} \tag{4}$$

$$P = \frac{Vi}{m} \tag{5}$$

where V is the voltage, i is the current, t is the time and m is the weight of electrode.

RESULTS AND DISCUSSION

The average weight, dimensions and density of GMs, CMs and ACMs (five duplicates monoliths) are listed in Table 1. Small change in the density of the samples after carbonization and activation of GMs and CMs, respectively, shown in this table, is resulted from a small different between the percentages of weight lost and volume shrinkage of the samples during such processes. The density value of ACMs around 1 g m^{-3} indicates that these samples are very porous. The percentage of porosity can be calculated from the equation, $porosity (\%) = \left[1 - \frac{\rho_{ACMs}}{\rho_{graphite}}\right] x100$, where ρ is the density of ACMs, $\rho_{graphite}$ is the theoretical density of graphite (2.268 g cm^{-3}). For the ACMs, the calculated percentage of porosity is 56.77%.

X-ray diffractogram for CMs and ACMs are shown in Figure 1. The presence of diffraction peaks (002) and (100) at 23.59° and 44.09° (CMs), 24.29° and 44.36° (ACMs), respectively, indicates that both CMs and ACMs have turbostratic structure [12, 13]. The values of d$_{002}$ and d$_{100}$ (calculated using Bragg equation [12]) and L$_c$ and L$_a$ (calculated using Scherrer equation [12]) from the peaks (002) and (100), respectively for the CMs and ACMs microcrytallites are shown in

Table 2. The values in this Table are typical for carbon from biomass precursor.

TABLE 1. Weight, dimension and density of GM, CM and ACM.

Samples	w(g)	t(mm)	d(mm)	$\rho(g\ cm^{-3})$
GM	0.74	2.27	20.16	1.01
CM	0.27	1.55	14.54	1.04
ACM	0.23	1.51	14.02	0.98

FIGURE 1. XRD pattern for CM and ACM.

TABLE 2. Interlayer spacing and crystallite dimensions for CM and ACM.

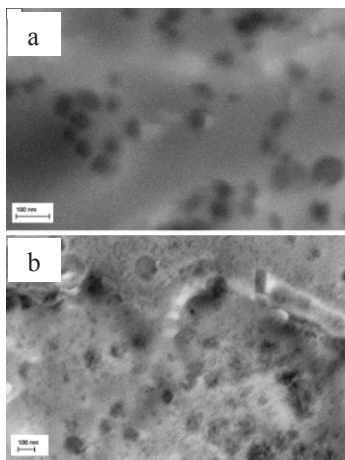| Samples	d_{002} (Å)	d_{100} (Å)	L_c (Å)	L_a (Å)
CM	3.76	2.05	10.12	30.44
ACM	3.66	2.04	12.60	42.13

FIGURE 2. FESEM Micrographs for (a) CM, (b) ACM.

FESEM micrographs, shown in Figure 2, for the (a) CMs and (b) ACMs with magnification of 100 kX (2.5 mm = 100 nm) clearly indicate that ACMs is more porous than CMs. This is an expected result because the CO_2 activation conducted on CMs for 4 hours was expected to create more pores. It will be seen later that this result is consistent with the N_2 adsorption-desorption isotherms data.

Figure 3 shows the N_2 adsorption-desorption isotherms plots for CM and ACM, which exhibit type I profile (IUPAC standard [14]), indicating that

dominant pores in both samples are micropores. As can be seen in Table 3, it was expected that ACM has significantly larger micropore volume than the non-activated sample (CM), and this result is consistent with the FESEM observation, and also can be correlated with the data in Table 2 [12]. The porosity characteristic shown in Table 3 is typical for commonly used activated carbon electrode for supercapacitor application [15, 16].
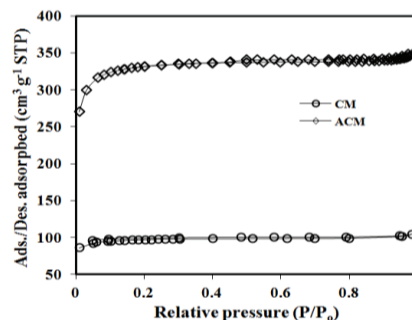

FIGURE 3. N_2 adsorption-desorption isotherms of CM and ACM at 77 K.

TABLE 3. Porosity data for CM and ACM.

Samples	CM	ACM
S_{BET} (m^2g^{-1})	293.948	1000.469
S_{Meso} (m^2g^{-1})	35.310	169.521
S_{Micro} (m^2g^{-1})	258.638	830.948
V_{Meso} (cm^3g^{-1})	0.027	0.062
V_{Micro} (cm^3g^{-1})	0.134	0.438
D (Å)	3.280	2.172

Nyquist plots of EIS data for the Cell(0.5), Cell(1.0) and Cell(1.5) are shown in Figure 4 (inset a). For all concentration, there are (i) a semicircle in high (ii) a straight line with a slope of around 45° (Warburg diffusion) in middle frequencies region, which represents mixed effects of resistive and capacitive, and (iii) an almost vertical line in lower frequencies region, which represents a purely capacitive affect. The curve appear to be very similar to each other but the data show a noticeable different in the values of imaginary impedance at the lowest recorded frequency (f_l = 0.01 Hz). The C_{sp} calculated using equation (1) and this f_l value, shown in Table 4, indicates that Cell (1.0) corresponds to a slightly higher C_{sp}. This result suggests that concentration of electrolyte in the range between 0.5 M and 1.5 M is around its optimum position in terms of allowing the highest mobility of ions to occupy pores of electrode to form double layer. A similar optimum behavior was observed for the Na_2SO_4 tested with binder based carbon electrode [6], H_2SO_4 tested with mesophase-pitch-based carbon electrode [9], KOH tested with carbon cryogel electrode [17].

In the Nyquist plots for the cell with KOH [17] and H_2SO_4 [18] electrolytes at different concentration,

respectively, it was observed that the value of Z' (real impedance) at the intercept on the real axis decreased as the concentration increased. The same trend is exhibited by our data in Figure 4, where the intercept gives the values of 0.679 Ω, 0.592 Ω and 0.535 Ω for the concentrations of 0.5, 1.0 and 1.5 M, respectively. The value at the intercept (R_s) is the sum of the contact resistance (between electrode and current collector) and the resistance of electrolyte.
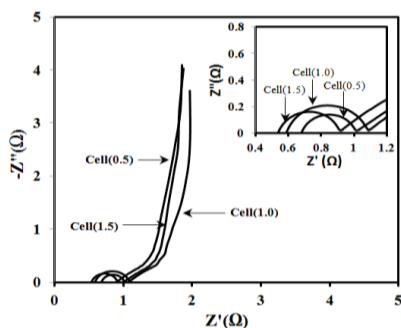

FIGURE 4. Nyquist plots for Cell(0.5), Cell(1.0) and Cell(1.5).

TABLE 4. Specific capacitance, specific energy and specific power for Cell(0.5), Cell(1.0) and Cell(1.5).

Molarity	Specific Capacitance ($F\ g^{-1}$)			Energy ($Wh\ kg^{-1}$)	Power ($W\ kg^{-1}$)
	EIS	CV	GCD		
0.5 M	144	150	203	5.29	172
1.0 M	161	153	206	5.79	174
1.5 M	141	140	201	5.26	171

CV data recorded within a potential range of 0.1 – 1.0 V, and with a scan rate of 5 mV/s for the Cell(0.5), Cell(1.0) and Cell(1.5), shown in Figure 5 (a), appear to have a rectangular like shape (without redox peak), indicating that in this range of electrolyte concentration, all cells are stable and exhibit a good capacitive behavior resulted purely from electrostatic charges transfer. The C_{sp} values calculated using equation (2) from the data in Figure 5(a) are shown in Table 4, and the C_{sp} values from the data with the scan rate at 1, 5, 25, 50 and 100 mV/s are shown in Figure 5(b), respectively. The C_{sp} value for the Cell(1.0) is slightly higher than other cells, but as can be seen in Figure 5(b), this trend changed when the scan rates are higher than 5 mV/s.

GCD curves recorded within potential range 0-1 V at a current density of 10 mA cm^{-2} for the Cell(0.5), Cell(1.0) and Cell(1.5) are shown in Figure 6. A slight different in the GCD curves between the different cells can be seen in this figure, with the Cell(1.0) exhibits only a slightly noticeable better performance than the other cells. This indicates that 0.5 M gap of electrolyte concentration between the cells is too small to generate a significant different on the cell performance. The C_{sp}

calculated from the data in Figure 6 using equation (3) is shown in Table 4. It can also be seen in this figure that for all the cells, there is a sudden drop in the potential at the beginning of the discharge curves, indicating that all cells have ohmic resistance [19].
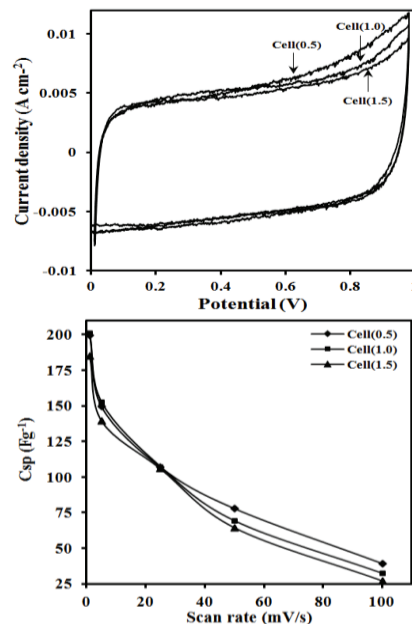

FIGURE 5(a). Cyclic voltammogram and (b) specific capacitance versus scan rate for Cell(0.5), Cell(1.0) and Cell(1.5).

Specific energy (E) and specific power (P) calculated from the discharge curves in Figure 6 using equations (4) and (5) is shown as a Ragone plots in Figure 7 [20]. This result shows that the Cell(1.0) has a better P-E relationship compared to the other cells, and it gives a maximum E at 174 Wkg^{-1}, corresponding to P at 5.79 Whkg^{-1} (Table 4). A similar optimum result at 1.0 M H_2SO_4 electrolyte was observed by Weng et al. [5].
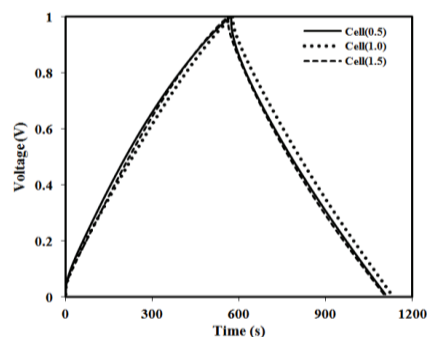

FIGURE 6. Galvanostatic charge-discharge curves for Cell(0.5), Cell(1.0) and Cell(1.5).

Table 5 shows the literature results of specific capacitance for different carbon electrodes tested in different type of electrolyte with different range of

concentration. The results in this table clearly demonstrate that there is a range of specific capacitance values within a range of its respective concentration. If the range of concentration is appropriately selected for a given electrode characteristic, it is expected that three would be an optimum concentration level that is corresponding to maximum specific capacitance value. As can be seen in our result, 1.0 M H_2SO_4 electrolyte seems to be optimum for the electrode produced in our study.
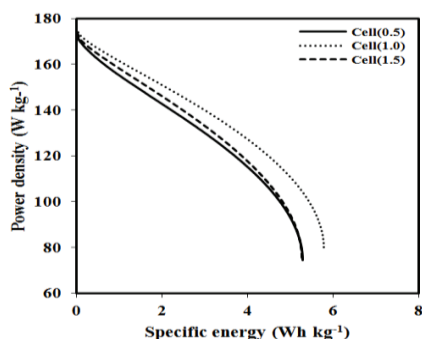

FIGURE 7. Ragone plots for Cell(0.5), Cell(1.0) and Cell(1.5).

TABLE 5. Specific capacitance, specific energy and specific power for different carbon electrodes with different range of electrolyte concentration.

Molarity	C_{sp} (F g^{-1})	E (Whkg^{-1})	P (Wkg^{-1})	Ref.
0.1 – 1 M (H_2SO_4)	12 – 15.95	-	-	[5]
0.1 – 1 M (Na_2SO_4)	74 - 86	5.33-5.64	-	[6]
1 – 18 M (H_2SO_4)	450	-	-	[9]
0.1 – 6 M (KOH)	7.37 - 8.37	-	-	[21]

CONCLUSION

ACMs prepared from the pre-carbonized EFB for application as electrodes of symmetrical supercapacitor cells were found to have a turbostratic structure and highly microporous characteristic. The fabricated cells with electrolyte concentrations of 0.5, 1.0 and 1.5 M, respectively were evaluated by the EIS, CV and GCD methods. All the methods found that 1.0 M electrolyte concentration consistently gave a slightly better supercapacitive performance than other concentration, and this optimum concentration generated the specific capacitance, maximum specific energy and maximum specific power values at 206 Fg^{-1}, 5.79 Wh kg^{-1} and 174 W kg^{-1}, respectively.

ACKNOWLEDGEMENTS

REFERENCES

1. M. Inagaki, H. Konnoa and O. Tanaike. *J. Power Sources* 195, 7880–7903 (2010).
2. B. McEnaney, "Structure and Bonding in Carbon Materials," in *Carbon Materials for Advanced Technologies*, edited by T.D. Burchell, Amster=dam: Elsevier Science Ltd. (1999) pp. 1-33.
3. A. G. Pandolfo and A. F. Hollenkamp, *J. Power Sources* 157, 11-27 (2006).
4. E. Taer, M. Deraman, I. A. Talib, Awitdrus, S.A. Hashmi, and A. A. Umar, *Int. J. Electrochem. Sci.* 6, 3301 – 3315 (2011).
5. T.W. Weng, W. Huang and K.Y. Lee, *Vacuum* 83, 629-632 (2009).
6. K.C. Tsay, L. Zhang and J. Zhang, *Electrochim. Acta* 60, 428– 436 (2012).
7. X. Zhang, X. Wang, L. Jiang, H. Wu, C. Wu and J. Su, *J. Power Sources* 216, 290-296 (2012)
8. P. M. Kulal, D.P. Dubal, C.D. Lokhande, V.J. Fulari, *J. Alloys Compd.* 509, 2567-2571 (2011).
9. Y. Soneda, M. Toyoda, Y. Tani, J. Yamashita, M. Kodama, H. Hatori and M. Inagaki, *J. Phys. and Chem. Solids* 65, 219-222 (2004).
10. M. Deraman, R. Omar, S. Zakaria, I.R. Mustapa, M. Talib and N. Alias, *J. Mater. Sci.* 37, 3329-3335 (2002).
11. C. Portet, P. L. Taberna, P. Simon, E. Flahaut and C. Laberty-Robert, *Electrochim. Acta* 50, 4174-4181 (2005).
12. Awitdrus, M. Deraman, I.A. Talib, R. Omar, M.H. Jumali, E. Taer and M.M. Saman, *Sains Malaysiana* 39, 83-86 (2010).
13. M. Deraman, S.K.M. Saat, M.M. Ishak, Awitdrus, E. Taer, I.A. Talib, R. Omar and M.H. Jumali, *AIP Conf. Proc. 1284*, 179-186 (2010).
14. M. Khalfaoui, S. Knani and M.A. Hachicha, A. Ben Lamine, *J. Colloid Interface Sci.* 263, 350-356 (2003).
15. K. Yang, J. Peng, C. Srinivasakannan, L. Zhang, H. Xia, X. Duan, *Bioresour. Technol.* 101, 6163-6169 (2010).
16. O. Iaonnidou and A. Zababiotou, *Renewable Sustainable Energy Rev.* 11, 1966-2005 (2007).
17. M.S. Song, S. Nahm and Y.J. Oh, *J. Kor. Ceram. Soc.* 45, 662-666 (2008).
18. W.G. Pell, B.E. Conway and N. Marincic, *J. Electroanal. Chem.* 491, 9-21 (2000).
19. C.T. Hseih and H. Teng, *Carbon* 40, 667-674 (2002).
20. E. Taer, M. Deraman, I.A. Talib, S.A. Hashmi and A.A. Umar, *Electrochim. Acta.* 56, 10217-10222 (2011).
21. Y. Tian, Z.Q. Li; H.-F. Xu, Y.-B. Wu, F.-L. Yang, *Acta Phys. Chim. Sin.* 24, 612-618 (2008).